Chemistry Letters, 2025, **54**, upaf053
https://doi.org/10.1093/chemle/upaf053
Advance access publication 12 March 2025

Letter

Calcination-driven Co^{4+} incorporation in hydrothermally synthesized $NaTaO_3$

Masato Yanagi[1], Juan Casanova-Cháfer[2], Takayoshi Hara[1], Yi-Hao Chew[3], Tomoko Yoshida[4], Hiroshi Onishi[3,5], Carla Bittencourt[2], Nobuyuki Ichikuni[1,*]

[1]Department of Applied Chemistry and Biotechnology, Graduate School of Science and Engineering, Chiba University, Yayoi-cho 1-33, Inage-ku, Chiba, Chiba 263-8522, Japan

[2]Chimie des Interactions Plasma-Surface (ChIPS), University of Mons, Mons 7000, Belgium

[3]Department of Chemistry, Graduate School of Science, Kobe University, Rokkodai, Nada-ku, Kobe, Hyogo 657-8501, Japan

[4]Department of Applied Energy, Graduate School of Engineering, Nagoya University, Furo-cho, Chikusa-ku, Nagoya, Aichi 464-8601, Japan

[5]Department of Materials Molecular Science, Electronic Structure, Division of Advanced Molecular Science, Institute for Molecular Science, Myodaiji, Okazaki, Aichi 444-8585, Japan

*Corresponding author: Department of Applied Chemistry and Biotechnology, Graduate School of Science and Engineering, Chiba University, Yayoi-cho 1-33, Inage-ku, Chiba, Chiba 263-8522, Japan. Email: ichikuni@faculty.chiba-u.jp

Abstract

A cobalt-doped sodium tantalate ($NaTaO_3$, NTO) catalyst was synthesized via a hybrid approach combining hydrothermal synthesis with a brief calcination step. Structural characterization through X-ray absorption spectroscopy and X-ray photoelectron spectroscopy revealed enhanced cobalt incorporation within the $NaTaO_3$ matrix following the calcination treatment. This finding was corroborated by catalytic performance evaluations during liquid-phase *p*-xylene oxidation. The Co 3s X-ray photoelectron spectroscopy analysis provided direct evidence of cobalt existing in the tetravalent oxidation state (Co^{4+}) within the host lattice, indicating successful substitution at tantalum sites.

Keywords: cobalt-doped $NaTaO_3$, valence of doped Co, X-ray analysis.

Graphical Abstract

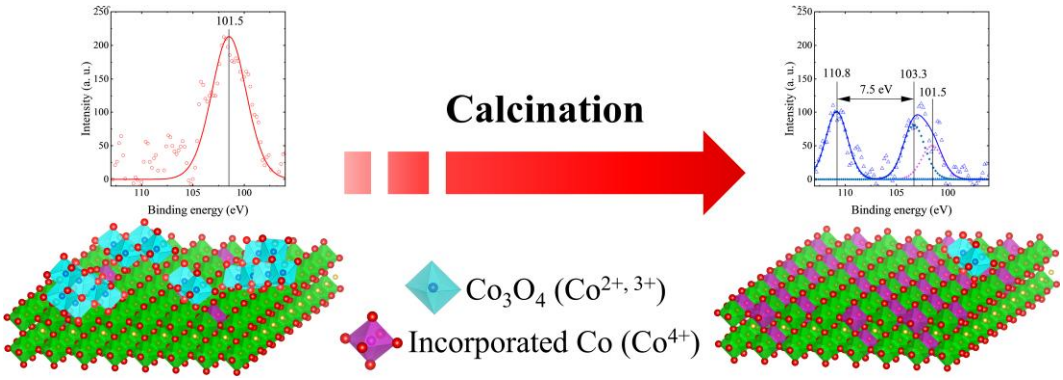

Cobalt possesses a relatively high oxidation ability among base metals and is used in various oxidation reactions. In particular, cobalt exhibits high catalytic activities comparable to that of precious metal catalysts in the oxidation of volatile organic compounds (VOCs) and carbon monoxide (CO).[1–4] In this point, cobalt is considered one of the most efficient catalysts in terms of cost and sustainability.[5] While cobalt is less active than precious metal catalysts in liquid-phase oxidation reactions, it has been used in certain alcohol oxidation reactions[6] and H-C(sp^3) oxidation reactions.[7,8] Since the leaching and aggregation of cobalt during the catalyzing process is a challenge in liquid-phase oxidation reactions, supports that can stably retain active species to prevent leaching and aggregation are required.

Perovskite-type oxides have been applied in various fields such as catalysts,[9] gas sensors,[10] semiconductors,[11] and solar

[Received on 10 February 2025; revised on 7 March 2025; accepted on 10 March 2025; corrected and typeset on 2 April 2025]

cells.[12] The general chemical formula of perovskite-type oxide is ABO_3, where the A site is occupied by relatively large radius metal cations (e.g. alkaline metals, alkaline earth metals, and lanthanides) and the B site is occupied by relatively small-radius metal cations, such as transition metals.[13] Perovskite-type oxides are known for their stability against heat and acids, and for the ion exchangeability at the A and B sites with other metal ions of similar ionic radii. These unique properties play an important role in catalytic use and a wide range of applications. For example, palladium-doped perovskite-type oxide catalysts have been used as excellent catalyst supports because they prevent aggregation and leaching of active species and extend catalyst lifetime.[14,15]

With reference to these examples, we designed a catalyst in which cobalt, an active species, is incorporated into perovskite-type oxides, aiming for applications in liquid-phase oxidation reactions. Our laboratory has previously synthesized sodium tantalate ($NaTaO_3$, NTO) catalysts with cobalt addition and applied it to the liquid-phase oxidation of *p*-xylene.[16] This paper clarified that the addition of cobalt enables ion exchange to occur during synthesis, and cobalt can be incorporated into the perovskite structure. The incorporation of metals with different valences into a perovskite structure typically leads to the generation of ionic defects, changes in metal valence, or both.[13] However, the electronic structure of cobalt in the NTO remains unclear. In addition, it has also shown that not all of the 1 wt% cobalt added is incorporated by hydrothermal synthesis.

In this study, we aim to determine the electronic structure of the incorporated cobalt, improve the synthesis method to increase the amount of incorporated cobalt.

Various methods exist for synthesizing NTO, including solid-state synthesis,[17] sol–gel methods,[18] and hydrothermal synthesis.[19] Among these, hydrothermal synthesis is widely used due to its low temperature and simplicity. However, hydrothermal synthesis provides a small amount of dopant in the structure, so we employed a hybrid synthesis method that combines hydrothermal synthesis with a brief calcination step—the calcination step after hydrothermal synthesis is expected to increase the amount of incorporated cobalt.

The hydrothermal synthesis method followed a previous study,[16] where the catalyst was prepared by hydrothermal synthesis at 453 K for 24 h with 1 wt% cobalt addition and denoted as Co-NTO_prist. The catalyst was then calcined at 973 K for 3 h to obtain the calcined catalyst (denoted as Co-NTO_973). For comparison, a conventional impregnation catalyst was also prepared using NTO, which was hydrothermally synthesized at 453 K for 24 h. Cobalt loading was regulated to 1 wt% and calcined at 573 K for 3 h to obtain the catalyst (imp Co/NTO_573).

Powder X-ray diffraction (XRD) of the prepared catalysts revealed that the NTO had an orthorhombic perovskite structure (space group: *Pcmn*), as reported in previous studies.[16,19,20] Clear peak shifts or structural changes were not observed in the hydrothermal catalysts with the addition of cobalt or calcination, due to the small amount of cobalt incorporated (<1 wt%). In addition, in the catalysts prepared by an impregnation method, no cobalt-related peaks were observed despite all the added cobalt being present on the catalyst surface, which may come from the low cobalt content. It is natural that no cobalt-related peaks are observed for hydrothermal catalysts because of the increased cobalt incorporated compared to impregnation catalysts.

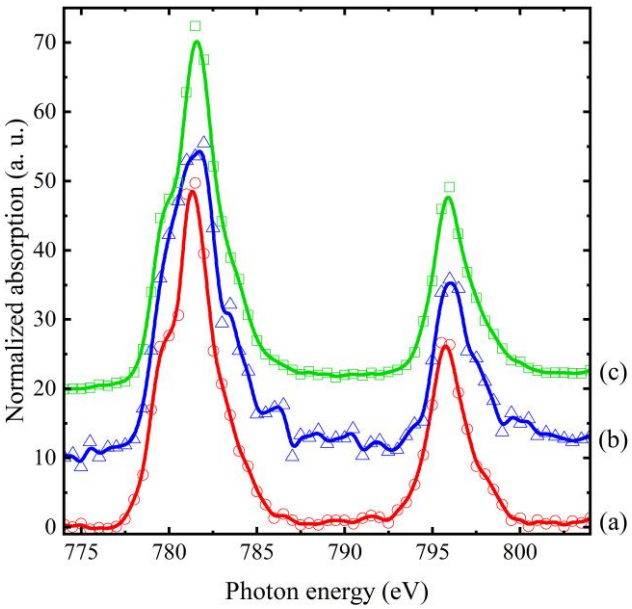

Fig. 1. Normalized Co $L_{2,3}$-edge XAS spectra of a) Co-NTO_prist, b) Co-NTO_973, c) imp Co/NTO_573.

To analyze the chemical species of the cobalt, soft X-ray absorption spectroscopy (XAS) measurement was carried out. The total electron yield method was applied, as it provides information that is relatively close to the surface. The Co $L_{2,3}$-edge XAS spectra are shown in Fig. 1. Hydrothermal catalyst (Fig. 1(a)) and impregnation catalyst (Fig. 1 (c)) exhibit a distinct shoulder around 780 eV. The shape of the spectra confirms that the main surface cobalt species is Co_3O_4.[21] On the other hand, the shoulder of the calcined catalyst (Fig. 1 (b)) around 780 eV becomes less distinct, and the $L_{2,3}$-edge peaks shift slightly to higher energy. In the literature,[21–23] it has been observed that the XAS $L_{2,3}$-edge spectra shift towards higher energies as the cobalt oxidation state increases. Therefore, the change in the peak shape observed in the calcination catalyst can be attributed to an increase in the incorporated cobalt species on the surface due to calcination at 973 K. In addition, the shift towards higher energies suggests that the incorporated cobalt has a higher oxidation state than Co_3O_4.

To confirm the chemical state of cobalt, X-ray photoelectron spectroscopy (XPS) measurement was performed. The energy was calibrated with reference to the adventitious carbon 1s peak (284.8 eV) in the sample. Wide-scan XPS spectra revealed that lower cobalt concentration of Co-NTO catalyst compared to that of imp Co/NTO_573 (Supplementary Fig. S1). This means existence of incorporated cobalt species in Co-NTO catalyst.

The Co 2p XPS spectra are shown in Fig. 2; the Co 2p doublet has a peak around 780 eV assigned to Co $2p_{3/2}$ and a peak around 795 eV assigned to Co $2p_{1/2}$. Each peak of the doublet is associated with a low-intensity satellite on the higher-energy side. The line profile and binding energy of the Co 2p peaks suggest that the main cobalt species present on the surface is Co_3O_4.[24,25] On the other hand, the Co2p spectrum of the calcined catalyst (Fig. 2 (b)) demonstrated a broadening and a shift towards higher binding energies. It is known that in the Co 2p XPS spectrum, the peaks shift towards higher binding energies as the cobalt valence

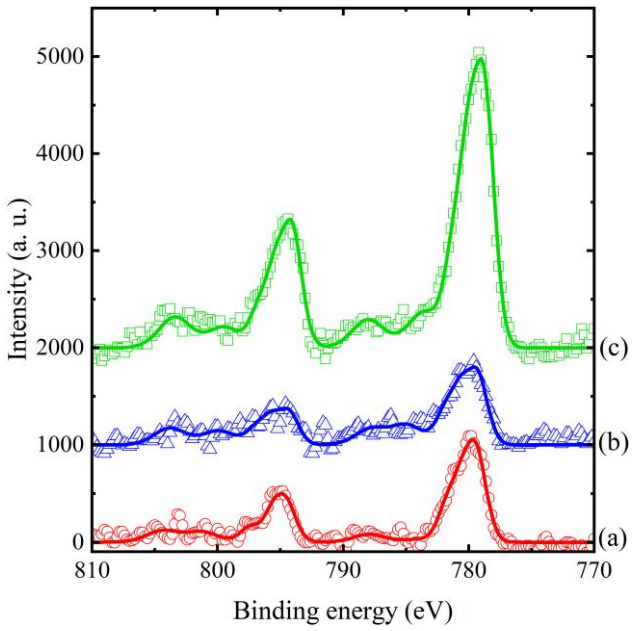

Fig. 2. Co 2p XPS spectra of a) Co-NTO_prist, b) Co-NTO_973, c) imp Co/NTO_573. The lines are only a guide for the eyes.

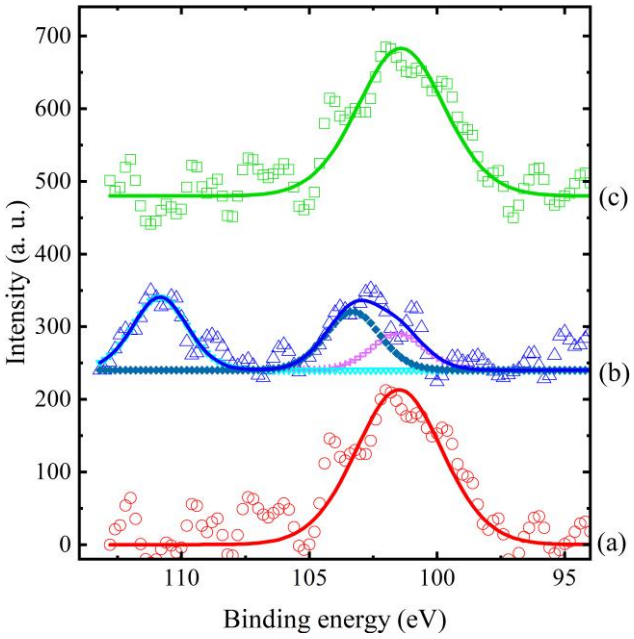

Fig. 3. Co 3s XPS spectra of a) Co-NTO_prist, b) Co-NTO_973, purple plus-mark represents the main peak of Co_3O_4 ($Co^{2+,\ 3+}$), dark-blue diamond-mark represents the main peak of incorporated cobalt (Co^{4+}), light-blue reverse-triangle-mark represents the exchange-splitting peak of incorporated cobalt. c) imp Co/NTO_573. The lines are only a guide for the eyes.

increases.[26] Thus, similar to the XAS results, this chemical shift can be attributed to an increase in the cobalt oxidation state compared to Co_3O_4.

To determine the oxidation state of the incorporated cobalt species, Co 3s XPS spectra were analyzed. Figure 3 shows the Co 3s spectra for each catalyst. The 3s peak in 3d transition metals undergoes exchange splitting, and the splitting width, ΔE_{3s}, is linearly related to the number of unpaired electrons in the 3d orbital.[27,28] Therefore, the valence of a metal can be estimated by comparing its splitting width with that of a standard sample. Table 1 shows the exchange splitting widths for representative cobalt species. The Co 3s peak for the hydrothermal catalyst (Fig. 3 (a)) and the impregnation catalyst (Fig. 3 (c)) did not exhibit any splitting, indicating that the predominant cobalt species on the catalyst surface is Co_3O_4. In contrast, the calcined catalyst (Fig. 3 (b)) had an exchange splitting of the 3s peak, and the lower binding energy peak broadened. This peak was deconvoluted into two distinct components; one component was identified as generated from photoelectrons emitted from cobalt atoms in Co_3O_4, suggesting the presence of Co_3O_4 that remains on the surface without being incorporated into the lattice. Given that Co_3O_4 does not undergo exchange splitting, the component centered at 103 eV is attributed to the exchange-splitting state. The higher-energy exchange-splitting peak is centered at 110.5 eV. Consequently, the calculated exchange-splitting width was determined to be 7.5 eV, which exceeds the corresponding value for CoF_3 containing Co^{3+}, indicating that the incorporated cobalt is in a higher oxidation state than Co^{3+}. To validate this measurement, the exchange-splitting width for Co^{4+} was predicted using the following equation and data presented in Table 1, which delineates the correlation between the exchange-splitting width, ΔE_{3s}, of the 3s peak and the number of unpaired electrons in the 3d orbitals.

Table 1. XPS exchange-splitting width of Co 3s peak.

Co species	ΔE_{3s} (eV)	Ref.
CoO	4.7	Brundle et al.[29]
$Co(OH)_2$	5.0	Brundle et al.[29]
CoF_2	5.0	Carver et al.[27]
CoF_3	6.0	Carver et al.[27]
Co_3O_4	No splitting	Brundle et al.[29]

$$\Delta E_{3s} = \frac{(2S+1)G^2(3s,\ 3d)}{2l+1}$$

S is the total spin of the 3d electrons, $G^2(3s, 3d)$ is the Slater exchange integral, and l ($l = 2$) is an azimuthal quantum number. Considering that exchange splitting does not occur for $3d^0$,[30] the exchange-splitting values of CoF_2 ($3d^3$) and CoF_3 ($3d^4$) from Table 1 were used for the estimation. Based on those data, the exchange-splitting width of Co^{4+} ($3d^5$) was determined to be 7.3 eV, which is in close agreement with the measured value. This confirms that the incorporated cobalt is in the Co^{4+} oxidation state, as indicated by the Co 3s XPS results.

To summarize the results of the analysis, the main cobalt species on the surface of hydrothermal catalysts is Co_3O_4, indicating that hydrothermal synthesis alone does not yield a sufficient amount of incorporated cobalt on the catalyst surface. In contrast, in the calcined catalyst, the amount of incorporated cobalt on the catalyst surface increased, and their oxidation state was identified as Co^{4+}. The reason of the incorporated cobalt species cannot be confirmed in the hydrothermal catalyst can be attributed to two factors: first, the cobalt that was not incorporated appeared as Co_3O_4, and second, relatively few cobalt species were incorporated on the surface during hydrothermal synthesis, as cobalt is incorporated both in bulk and on the surface. In the present synthesis method, the

Table 2. Results of the *p*-xylene oxidation reaction.

Catalyst	Amount[a] (mmol)	Selectivity (%)		
		PMAL	PTALD	PTA
NTO	0.03	0.0	85.4	14.6
Co-NTO_prist	0.39	18.8	70.2	11.0
Co-NTO_973	0.36	13.0	78.1	8.9
imp Co/NTO_573	0.53	19.7	61.9	18.4

Reaction condition: *p*-xylene (3 mL), Cat. (25 mg), O_2 atmosphere (1 atm), 393 K, 6 h.
[a]Total product amount.

Co_3O_4 that was not fully incorporated during hydrothermal synthesis was incorporated into the NTO perovskite structure through calcination. This process increased the proportion of incorporated cobalt species on the catalyst surface, facilitating the formation of a more suitable surface structure for catalysis.

To confirm this hypothesis, a liquid-phase oxidation reaction of *p*-xylene was carried out under the conditions of 1 atm oxygen atmosphere, 393 K, 6 h. The results are shown in Table 2. Co-NTO_prist and imp Co/NTO_573, in which the main surface cobalt species is Co_3O_4, had similar *p*-methylbenzyl alcohol (**PMAL**) selectivity. On the other hand, the selectivity of Co-NTO_973 for both **PMAL** and *p*-toluic acid (**PTA**) decreased, while the selectivity for *p*-tolualdehyde (**PTALD**) improved. Given the results of the previous report,[16] the improvement in **PTALD** selectivity observed in Table 2 can be attributed to an increase in the amount of incorporated cobalt.

In conclusion, the combined XAS and XPS analysis demonstrate that the hybrid synthesis method involving a brief calcination step following hydrothermal synthesis enhances cobalt incorporation within the NTO perovskite structure at the catalyst surface. Furthermore, Co 3s XPS analysis reveals that the incorporated cobalt exists in the Co^{4+} oxidation state, confirming substitution at tantalum sites.

Acknowledgments

This study was also supported by the Joint Usage/Research Center for Catalysis (Proposal#23DS0487). XAS data were collected at BL4B of UVSOR, IMS (24IMS6638). The authors thank Dr. Hiroshi Iwayama for the assistance in carrying out XAS measurements. The figure of the Graphical Abstract was drawn by VESTA software.[31]

Supplementary data

Supplementary material is available at *Chemistry Letters* online.

Funding

This work was financially supported by a Grant-in-Aid for Scientific Research from the Japan Society for the Promotion of Science (JSPS KAKENHI, 22K04822). C. B. is a research associate of FNRS, Belgium.

Conflict of interest statement. None declared.

References

1. F. Wyrwalski, J. Giraudon, J. Lamonier, *Catal. Lett.* **2010**, *137*, 141. https://doi.org/10.1007/s10562-010-0356-6
2. Y. Yu Yao, *J. Catal.* **1974**, *33*, 108. https://doi.org/10.1016/0021-9517(74)90250-4
3. X. Xie, Y. Li, Z. Liu, M. Haruta, W. Shen, *Nature* **2009**, *458*, 746. https://doi.org/10.1038/nature07877
4. L. Hu, K. Sun, Q. Peng, B. Xu, Y. Li, *Nano Res.* **2010**, *3*, 363. https://doi.org/10.1007/s12274-010-1040-2
5. L. F. Liotta, H. Wu, G. Pantaleo, A. M. Venezia, *Catal. Sci. Technol.* **2013**, *3*, 3085. https://doi.org/10.1039/c3cy00193h
6. J. Zhu, K. Kailasam, A. Fischer, A. Thomas, *ACS Catal.* **2011**, *1*, 342. https://doi.org/10.1021/cs100153a
7. C. Liang, X. Li, D. Su, Q. Ma, J. Mao, Z. Chen, Y. Wang, J. Yao, H. Li, *Mol. Catal.* **2018**, *453*, 121. https://doi.org/10.1016/j.mcat.2018.05.005
8. A. Aguadero, H. Falcon, J. M. Campos-Martin, S. M. Al-Zahrani, J. L. G. Fierro, J. A. Alonso, *Angew. Chem. Int. Ed.* **2011**, *50*, 6557. https://doi.org/10.1002/anie.201007941
9. K. Kamata, *Bull. Chem. Soc. Jpn.* **2019**, *92*, 133. https://doi.org/10.1246/bcsj.20180260
10. S. S. Patil, B. M. Babar, D. Y. Nadargi, F. I. Shaikh, J. D. Nadargi, B. R. Sankapal, I. S. Mulla, M. S. Tamboli, N. T. Nguyen Truong, S. S. Suryavanshi, *ACS Omega* **2024**, *9*, 29994. https://doi.org/10.1021/acsomega.4c00334
11. H. He, Z. Yang, Y. Xu, A. T. Smith, G. Yang, L. Sun, *Nano Converg.* **2020**, *7*, 32. https://doi.org/10.1186/s40580-020-00242-7
12. A. Bera, K. Wu, A. Sheikh, E. Alarousu, O. F. Mohammed, T. Wu, *J. Phys. Chem. C* **2014**, *118*, 18494. https://doi.org/10.1021/jp509753p
13. S. Royer, D. Duprez, F. Can, X. Courtois, C. Batiot-Dupeyrat, S. Laassiri, H. Alamdari, *Chem. Rev.* **2014**, *114*, 10292. https://doi.org/10.1021/cr500032a
14. Y. Nishihata, J. Mizuki, T. Akao, H. Tanaka, M. Uenishi, M. Kimura, T. Okamoto, N. Hamada, *Nature* **2002**, *418*, 164. https://doi.org/10.1038/nature00893
15. L. Saputra, T. Kojima, T. Hara, N. Ichikuni, S. Shimazu, *Mol. Catal.* **2018**, *453*, 132. https://doi.org/10.1016/j.mcat.2018.04.023
16. J. Wang, T. Hara, N. Ichikuni, *Chem. Lett.* **2024**, *53*, upae061. https://doi.org/10.1093/chemle/upae061
17. A. Yamakata, T. Ishibashi, H. Kato, A. Kudo, H. Onishi, *J. Phys. Chem. B* **2003**, *107*, 14383. https://doi.org/10.1021/jp036473k
18. C. Hu, C. Tsai, H. Teng, *J. Am. Ceram. Soc.* **2009**, *92*, 460. https://doi.org/10.1111/j.1551-2916.2008.02869.x
19. X. Li, J. Zang, *J. Phys. Chem. C* **2009**, *113*, 19411. https://doi.org/10.1021/jp907334z
20. P. Jana, V. A. de la, P. O'Shea, C. M. Montero, P. Galvez, P. Pizarro, J. M. Coronado, D. P. Serrano, *Green Chem.* **2015**, *17*, 1735. https://doi.org/10.1039/C4GC02064B
21. Y. Huang, W. Chen, Z. Xiao, Z. Hu, Y. Lu, J. Chen, C. Chen, H. Lin, C. Chen, K. T. Arul, S. Wang, C. Dong, W. Chou, *J. Phys. Chem. Lett.* **2022**, *13*, 8386. https://doi.org/10.1021/acs.jpclett.2c01557
22. T. Mizokawa, Y. Wakisaka, T. Sudayama, C. Iwaki, K. Miyoshi, J. Takeuchi, H. Wadati, D. G. Hawthorn, T. Z. Regier, G. A. Sawatzky, *Phys. Lett.* **2013**, *111*, 056404. https://doi.org/10.1103/PhysRevLett.111.056404
23. T. Matsushita, M. Mizumaki, N. Ikeda, M. Nakazawa, A. Agui, Y. Saitoh, T. Nakatani, A. Yoshigoe, S. Nakamura, *Surf. Rev. Lett.* **2002**, *9*, 1327. https://doi.org/10.1142/S0218625X02003755
24. M. C. Biesinger, B. P. Payne, A. P. Groosvenor, L. W. M. Lau, A. R. Gerson, R. St, C. Smart, *Appl. Surf. Sci.* **2011**, *257*, 2717. https://doi.org/10.1016/j.apsusc.2010.10.051
25. M. Oku, K. Hirokawa, *J. Electron Spectrosc. Relat. Phenom.* **1976**, *8*, 475. https://doi.org/10.1016/0368-2048(76)80034-5

26. S. Chowdhury, A. Jana, A. K. Mandal, R. J. Choudhary, D. M. Phase, *ACS Appl. Electron. Mater.* **2021**, *3*, 3060. https://doi.org/10.1021/acsaelm.1c00290
27. J. C. Carver, G. K. Schweitzer, T. A. Carlson, *J. Chem. Phys.* **1972**, *57*, 973. https://doi.org/10.1063/1.1678348
28. J. H. V. Vleck, *Phys. Rev.* **1934**, *45*, 405. https://doi.org/10.1103/PhysRev.45.405
29. C. R. Brundle, T. J. Chuang, D. W. Rice, *Surf. Sci.* **1976**, *60*, 286. doi:https://doi.org/10.1016/0039-6028(76)90318-6
30. P. Petzoldt, M. Eder, S. Mackewicz, M. Blum, T. Kratky, S. Günther, M. Tschurl, U. Heiz, B. A. J. Lechner, *J. Phys. Chem. C* **2022**, *126*, 16127. https://doi.org/10.1021/acs.jpcc.2c03851
31. K. Momma, F. Izumi, *J. Appl. Cryst.* **2011**, *44*, 1272. https://doi.org/10.1107/S0021889811038970